
Article:
Watson, David Mark, Hartley, Tom orcid.org/0000-0002-4072-6637 and Andrews, Timothy John orcid.org/0000-0001-8255-9120 (2017) Patterns of response to scrambled scenes reveal the importance of visual properties in the organization of scene-selective cortex. Cortex. ISSN 1973-8102

https://doi.org/10.1016/j.cortex.2017.04.011

Accepted Manuscript

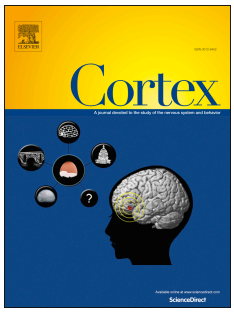

Patterns of response to scrambled scenes reveal the importance of visual properties in the organization of scene-selective cortex

David M. Watson, Tom Hartley, Timothy J. Andrews

PII: S0010-9452(17)30128-4

DOI: 10.1016/j.cortex.2017.04.011

Reference: CORTEX 1997

To appear in: *Cortex*

Received Date: 15 November 2016

Revised Date: 3 March 2017

Accepted Date: 11 April 2017

Please cite this article as: Watson DM, Hartley T, Andrews TJ, Patterns of response to scrambled scenes reveal the importance of visual properties in the organization of scene-selective cortex, *CORTEX* (2017), doi: 10.1016/j.cortex.2017.04.011.

PATTERNS OF RESPONSE TO SCRAMBLED SCENES REVEAL THE IMPORTANCE OF VISUAL PROPERTIES IN THE ORGANIZATION OF SCENE-SELECTIVE CORTEX

David M. Watson, Tom Hartley, Timothy J. Andrews*

Department of Psychology and York Neuroimaging Centre,

University of York, York, YO10 5DD, United Kingdom

* Corresponding author: timothy.andrews@york.ac.uk

Key words: Scene, Cortex, Category, PPA, RSC, OPA, topographic

ABSTRACT

Neuroimaging studies have found distinct patterns of neural response to different categories of scene in scene-selective regions of the human brain. However, it is not clear how information about scene category is represented in these regions. Images from different categories vary systematically in their visual properties as well as their semantic category. So, it is possible that patterns of neural response could reflect variation in visual properties. To address this question, we used fMRI to measure patterns of neural response to intact and scrambled scene categories. Although scrambling preserved many of their visual characteristics, perception of scene categories was severely impaired. Nevertheless, we found distinct patterns of response to different scene categories in the parahippocampal place area (PPA) and the occipital place area (OPA) for both intact and scrambled scenes. Moreover, intact and scrambled scenes produced highly similar patterns of response. Our finding that reliable and distinct patterns of response in scene-selective regions are still evident when categorical perception is impaired suggests that visual properties play an important role in the topographic organization of these regions.

INTRODUCTION

The ability to perceive and recognize the spatial layout of visual scenes is essential for spatial navigation. Neuroimaging studies have identified a number of regions in the human brain that respond selectively to visual scenes (Epstein, 2008). For example, the parahippocampal place area (PPA) is a region on the ventral surface of the temporal lobe that displays preferential activity to images of scenes over and above images of objects and faces (Aguirre, Zarahn, & D'Esposito, 1998; Epstein & Kanwisher, 1998). Other place selective regions include the retrosplenial complex (RSC) located immediately superior to the PPA and the transverse occipital sulcus (TOS) or occipital place area (OPA) on the lateral surface of the occipital lobe (Dilks, Julian, Paunov, & Kanwisher, 2013). Damage to these regions leads to specific impairments in scene perception and spatial navigation (Aguirre & D'Esposito, 1999; Mendez & Cherrier, 2003).

Despite the importance of scene-selective regions for spatial navigation, the functional organisation of these regions remains unclear (Lescroart, Stansbury, & Gallant, 2015; Groen et al., 2017). For example, although scene-selective regions show distinct patterns of response to images of different scene categories (Walther, Caddigan, Fei-Fei, & Beck, 2009; Watson, Hartley, & Andrews, 2014), the basic organizing principles are unresolved. Some studies have argued that scene-selective regions represent information about 'high-level' semantic properties of natural scenes (Huth, Nishimoto, Vu, & Gallant, 2012; Stansbury, Naselaris, & Gallant, 2013; Walther et al., 2009; Walther, Chai, Caddigan, Beck, & Fei-Fei, 2011). This conclusion has, however, been challenged by other studies that have suggested that the patterns of response in scene-selective regions are better explained by properties of the scene, such as openness (Kravitz, Peng, & Baker, 2011; Park, Brady,

Greene, & Oliva, 2011) or distance (Amit, Mehoudar, Trope, & Yovel, 2012; Park, Konkle, & Oliva, 2015) rather than by semantic category.

Although concepts such as openness or distance provide plausible 'mid-level' dimensions with which to understand the organization of scene-selective regions, it is not clear whether they can be explained at an even more basic level in terms of low-level visual properties that co-vary with these properties (Oliva & Torralba, 2001). In recent studies, we have shown that variance in the patterns of response to different scene categories can be explained by corresponding variance in the image properties of the scenes (Andrews, Watson, Rice, & Hartley, 2015; Watson et al., 2014; Watson, Hymers, Hartley, & Andrews, 2016). These findings are consistent with previously reported biases in scene-selective regions for orientation (Nasr, Echavarria, & Tootell, 2014; Nasr & Tootell, 2012), spatial frequency (Musel et al., 2014; Rajimehr, Devaney, Bilenko, Young, & Tootell, 2011) and visual field location (Arcaro, McMains, Singer, & Kastner, 2009; Golomb & Kanwisher, 2012; Levy, Hasson, Avidan, Hendler, & Malach, 2001; Silson, Chan, Reynolds, Kravitz, & Baker, 2015) and provide further evidence for the role of image properties in the organization of scene-selective regions. However, a fundamental problem is that images drawn from the same scene category or with the same spatial layout are likely to have similar visual properties (Oliva & Torralba, 2001). So, reliable patterns of response are expected under high-level, mid-level and low-level accounts of scene perception.

The aim of this study was to directly determine the extent to which the patterns of neural response across scene-selective regions can be explained by selectivity to more basic properties of the stimulus. To address this question, we measured the neural response across scene-selective regions to intact images of different scene categories, as well as versions of these images that had been phase-scrambled at a global or local level. Our

rationale for using scrambled images is that they have many of the visual properties found in intact images, but disrupt perception of categorical and semantic information (Andrews, Clarke, Pell, Hartley, 2010; Coggan, Liu, Baker, & Andrews, 2016; Loschky et al., 2007; Loschky, Hansen, Sethi, & Pydimarri, 2010). Applying scrambling both locally and globally allowed us to further investigate the importance of the spatial properties of scenes to the neural response, as local scrambling better preserves the coarse-scale spatial arrangement of visual features in the original image. Our hypothesis was that, if scene-selective regions are sensitive to the visual differences between scene categories, then we would expect to find similar patterns of neural response to these categories even when images are scrambled.

METHODS

Participants

20 participants (5 males; mean age: 25.85; age range: 19-34) took part in the experiment. All participants were neurologically healthy, right-handed, and had normal or corrected-to-normal vision. Written consent was obtained for all participants and the study was approved by the York Neuroimaging Centre Ethics Committee.

Stimuli

Participants viewed scene images in two independent runs, one to localize the scene-selective regions, the other to experimentally investigate the effects of local and global scrambling manipulations. Images presented in the experiment runs were taken from the LabelMe database (http://cvcl.mit.edu/database.htm; Oliva & Torralba, 2001). Images for the localiser run were taken from the SUN database (http://groups.csail.mit.edu/vision/SUN/; Xiao, Hays, Ehinger, Oliva, & Torralba, 2010). Stimuli were presented using PsychoPy (Peirce, 2007, 2009) and were back-projected onto a custom in-bore acrylic screen at a distance of approximately 57 cm from the participant, with all images presented at a resolution of 256x256 pixels subtending approximately 10.7° of visual angle.

The image set for the main experiment comprised 180 greyscale images from 5 scene categories: city, coast, forest, indoor, and mountain (36 images per category). Each image was shown at 3 levels of image scrambling: intact, locally scrambled, and globally scrambled. Globally scrambled images were created by randomising the phase of the 2D frequency components across the whole image while keeping the magnitude constant.

Locally scrambled images were created by the same process, except that scrambling was applied independently within each of 64 windows of an 8x8 grid across the image. Luminance histograms across all images in all conditions were normalised using the SHINE toolbox (Willenbockel et al., 2010). Examples of the stimuli used in each condition are shown in Figure 1. Corresponding Fourier amplitude spectra plots are shown in Supplementary Figure 1. In order to assess the impact of the scrambling process on the visual similarity of the scene categories, we assessed the visual statistics of the images using the GIST descriptor (Oliva & Torralba, 2001). This generates a vector for each image describing the spectral energy at assorted spatial frequencies, orientations, and spatial positions within the image. We employed 32 filters spanning 8 orientations and 4 spatial frequencies, within 64 windows of an 8x8 spatial grid, yielding vectors of 2048 values. These vectors were then correlated within- and between-categories using a leave-one-image-out cross-validation procedure for each scrambling condition independently (Supplementary Figure 2a). The resulting similarity matrices are shown in Supplementary Figure 2a. We next tested the ability to distinguish scene categories based on this visual information by contrasting the within- over the between-category correlations (Supplementary Figure 2b). Significantly greater within- than between-category correlations were observed for the intact ($t(35) = 29.44$, $p < .001$, Cohen's $d = 4.91$), locally scrambled ($t(35) = 25.57$, $p < .001$, Cohen's $d = 4.26$), and globally scrambled scenes ($t(35) = 18.69$, $p < .001$, Cohen's $d = 3.11$). Thus, the scene categories remained visually distinct under all conditions of scrambling.

The localiser images comprised a separate set of 64 scene images plus their phase scrambled counterparts (128 images total), with all images presented in full colour. Images were chosen in approximately equal number from categories of indoor-manmade, outdoor-

manmade, and outdoor-natural scenes as these represent the 3 top-level branches of the SUN database hierarchy. Fourier-scrambled images were created by randomising the phase of the 2D frequency components in each colour channel of the original image while keeping the magnitude constant. Mean luminance was then equated across images.

[Figure 1 near here]

fMRI Experimental Design

During the experimental runs participants viewed images from the 5 scene categories. Images from each level of image scrambling were presented across separate experiment runs. For all participants, globally scrambled images were presented in the first run, locally scrambled in the second run, and intact images in the third run. This order was chosen as it was crucial to ensure that responses to scrambled scenes could not be primed by earlier viewing of the intact versions.

In each run, images from each category were presented in a blocked design. There were 6 images in each block. Each image was presented for 750ms followed by a 250ms grey screen that was equal in mean luminance to the scene images. Each stimulus block was separated by a 9s period in which the same grey screen as used in the inter-stimulus interval was presented. Each condition was repeated 6 times (total 30 blocks) in each run. To maintain attention throughout the experimental runs, participants had to detect the presence of a red dot randomly superimposed on one of the images in each block, responding via a button press.

To define scene-selective regions, independent data was collected while participants viewed images from 2 stimulus conditions (intact scenes, scrambled scenes). Images from each condition were presented in a blocked fMRI design, with each block comprising 9

144 images. Each condition was repeated 8 times (16 blocks). In each stimulus block, an image
145 was presented for 750ms followed by a 250ms grey screen. Each stimulus block was
146 separated by a 9s period in which a grey screen was presented. Participants performed a
147 one-back task that involved pressing a button when they detected a repeated image in each
148 block.
149
150 *Imaging Parameters*
151 All scanning was conducted at the York Neuroimaging Centre (YNiC) using a GE 3 Tesla HDx
152 Excite MRI scanner. Images were acquired with an 8-channel phased-array head coil tuned
153 to 127.72MHz. Data were collected from 38 contigual axial slices in an interleaved order via
154 a gradient-echo EPI sequence (TR = 3s, TE = 32.5ms, FOV = 288x288mm, matrix size =
155 128x128, voxel dimensions = 2.25x2.25 mm, slice thickness = 3mm with no inter-slice gap,
156 flip angle = 90°, phase-encoding direction = anterior-posterior, pixel bandwidth = 39.06 kHz).
157 In order to aid co-registration to structural images, T1-weighted in-plane FLAIR images were
158 acquired (TR = 2.5s, TE = 9.98ms, FOV = 288x288mm, matrix size = 512x512, voxel
159 dimensions = 0.56x0.56 mm, slice thickness = 3mm, flip angle = 90°). Finally, high-resolution
160 T1-weighted structural images were acquired (TR = 7.96ms, TE = 3.05ms, FOV =
161 290x290mm, matrix size = 256x256, voxel dimensions = 1.13x1.13 mm, slice thickness =
162 1mm, flip angle = 20°).
163
164 *fMRI Analysis*
165 Univariate analyses of the fMRI data were performed with FEAT v5.98
166 (http://www.fmrib.ox.ac.uk/fsl). In all scans the initial 9s of data were removed to reduce

the effects of magnetic stimulation. Motion correction (MCFLIRT, FSL; Jenkinson, Bannister, Brady, & Smith, 2002) was applied followed by temporal high-pass filtering (Gaussian-weighted least-squared straight line fittings, sigma=15s). Spatial smoothing (Gaussian) was applied at 6mm FWHM to both the localiser and experiment runs, in line with previous studies employing smoothing in conjunction with MVPA (Op de Beeck, 2010; Watson et al., 2014). Parameter estimates were generated for each condition by regressing the hemodynamic response of each voxel against a box-car convolved with a single-gamma HRF. Next, individual participant data were entered into higher-level group analyses using a mixed-effects design (FLAME, FSL). Functional data were first co-registered to an in-plane FLAIR anatomical image then to a high-resolution T1-anatomical image, and finally onto the standard MNI brain (ICBM152).

Scene selective regions of interest (ROIs) were defined from the localiser data of both experiments. ROIs were defined for the parahippocampal place area (PPA), retrosplenial complex (RSC), and occipital place area (OPA) that have been reported in previous fMRI studies (Dilks et al., 2013; Epstein & Kanwisher, 1998; Maguire, 2001). The locations of these ROIs were consistent with those reported in previous literature – see Supplementary Table 1. Within the MNI-2x2x2mm space, seed points were defined at the peak voxels within the intact>scrambled statistical map for each region (PPA, RSC, OPA) in each hemisphere. For a given seed, a flood fill algorithm was used to identify a cluster of spatially contiguous voxels around that seed which exceeded a given threshold. This threshold was then iteratively adjusted till a cluster size of approximately 500 voxels was achieved (corresponding to a volume of 4000mm^3); actual cluster sizes ranged from 499-502 voxels as an optimal solution to the algorithm was not always achievable. This step ensures that estimates of multi-voxel pattern similarity are not biased by the different sizes of ROIs

191 being compared. Clusters were combined across hemispheres to yield 3 ROIs, each
192 comprising approximately 1000 voxels. These regions are shown in Supplementary Figure 3,
193 and MNI co-ordinates of the seeds are given in Table 1. For comparison, we defined two
194 alternative versions of each of the scene ROIs using the same clustering method, based
195 upon independent localiser data from other experiments (not reported here). Specifically,
196 regions were defined using responses from contrasts of 1) Scenes > Faces, and 2) Scenes >
197 Objects. The locations of these regions are shown in Supplementary Figure 8, and MNI co-
198 ordinates of the seeds are given in Supplementary Table 2. In addition, a V1 control ROI was
199 defined from a recent standard atlas of retinotopic regions (Wang, Mruczek, Arcaro, &
200 Kastner, 2015).

201 Next, we measured patterns of response to different stimulus conditions in each
202 ROI. Parameter estimates were generated for each condition in the experimental scans.
203 The reliability of response patterns was tested using a leave-one-participant-out (LOPO)
204 cross-validation paradigm (Poldrack, Halchenko, & Hanson, 2009; Shinkareva et al., 2008) in
205 which parameter estimates were determined using a group analysis of all participants
206 except one. This generated parameter estimates for each scene condition in each voxel.
207 This LOPO process was repeated such that every participant was left out of a group analysis
208 once. These data were then submitted to correlation-based pattern analyses (Haxby et al.,
209 2001; Haxby, Connolly, & Guntupalli, 2014) implemented using the PyMVPA toolbox
210 (http://www.pymvpa.org/; Hanke et al., 2009). Parameter estimates were normalised by
211 subtracting the voxel-wise mean response across all experimental conditions (Haxby et al.,
212 2001). For each iteration of the LOPO cross-validation, the normalized patterns of response
213 to each stimulus condition were correlated between the group and the left-out participant.

This allowed us to determine whether there are reliable patterns of response that are consistent across individual participants.

Statistical Analyses

A Fisher's z-transform was applied to the correlation similarity matrices before further statistical analyses. We tested whether scene categories could be distinguished on the basis of the pattern of activity within each region to under each level of image scrambling. For each iteration of the LOPO cross-validation, we calculated an average within-category (on-diagonal) and an average between-category (off-diagonal) value across categories. These values were then entered into a paired-samples t-test. If scene category can be discriminated based on the pattern of activity it elicits, then significantly greater within- than between-category correlations would be expected. For the scene regions, a Bonferroni-Holm correction for multiple comparisons was applied across the 3 regions (PPA, RSC, OPA) and 3 scrambling conditions (intact, locally scrambled, globally scrambled). The V1 ROI represents a control analysis and hence was handled separately; here a Bonferroni-Holm correction for multiple comparisons was applied across the 3 scrambling conditions. A possible caveat here is that the leave-one-out procedure means that samples from each iteration are not truly independent, potentially violating the statistical assumptions of the t-test. To address this we repeated these analyses using a sign-flip permutation test on the differences between the scores. The results of these analyses closely followed those of the parametric t-tests – see Supplementary Table 3.

Next, we conducted a series of representational similarity analyses (RSAs; Kriegeskorte, Mur, & Bandettini, 2008) to investigate effects of different levels of scrambling. Correlation matrices were averaged across iterations of the cross-validation.

Representational similarity was assessed by correlating the off-diagonal elements of the averaged similarity matrices between the intact and locally scrambled conditions, and between the intact and globally scrambled conditions. If the scrambling does not abolish the pattern of relative similarity between categories relative to the intact condition, then a significant positive correlation would be expected between the intact and corresponding scrambled matrices. For the scene regions, a Bonferroni-Holm correction was applied across the 3 regions (PPA, RSC, OPA) and 2 analyses (intact versus locally scrambled, intact versus globally scrambled). The V1 ROI represents a control analysis and hence was handled separately; here a Bonferroni-Holm correction for multiple comparisons was applied across the 2 analyses.

To test for effects outside our ROIs, we also performed a series of whole-brain searchlight analyses (Kriegeskorte, Goebel, & Bandettini, 2006). A spherical ROI (6mm radius) was iterated over the whole-brain volume, and the MVPA repeated within each sphere. Decoding and representational similarity analyses were conducted in the same manner as for the ROI analyses. For the decoding analysis, for a given sphere an average within- and between-category correlation value was calculated for each LOPO iteration, and then a paired-samples t-test used to test the within > between difference across LOPO iterations. For the representational similarity analyses, for a given sphere the correlation matrices were averaged across LOPO iterations and the off-diagonal elements correlated between the scrambling conditions. In both cases, the p-value of the test was then assigned to the central voxel of the sphere.

Behavioural Experiment

We also tested the ability of participants to recognise the scenes under each level of image scrambling. An independent set of 18 participants naive to the purposes of the study were recruited (6 males; mean age: 21.7; age range: 19-39). Written consent was obtained for all participants and the study was approved by the University of York Psychology Department Ethics Committee. Each participant viewed a subset of 1/6th of the image set comprising 6 images from each category. Subsets were counterbalanced across participants. Participants viewed each image under all three levels of scrambling. Crucially, to prevent priming effects, participants viewed globally scrambled images first, followed by locally scrambled images, and finally intact images (as per the fMRI experiment). In each trial participants were shown an image for 750ms, and were then prompted to describe the type of scene they thought was shown, typing their responses. The stimulus duration was chosen to match that of the fMRI experiment. Participants were free to provide any description they wanted, and were also informed that they did not have to give a response if they could not reasonably see what type of scene was depicted. Accuracy was coded manually by two independent raters (both authors of the study). A correct response was defined as any which could reasonably be seen to accurately describe the corresponding intact scene, while an incorrect response was defined as one that did not accurately describe the intact scene or where no response was given. Accuracies were converted to proportions and an arcsine square-root transform was applied prior to further statistical tests. If participants did provide a description, they were next prompted to provide a confidence rating of their decision on a 7 point scale (not at all confident - very confident). No confidence ratings were collected for trials where participants did not provide descriptive responses. Participants were not provided with any information about the scene categories prior to the experiment – this was necessary in

order to match the design of the fMRI experiment, where participants were not provided with any information about the structure of the stimulus set beforehand either.

RESULTS

Behavioural Experiment

We tested the effects of the different levels of scrambling on participants' ability to recognise the scenes. Two independent raters (both authors) coded the descriptive responses for accuracy. Inter-rater reliability was high across the subjects (mean Cohen's kappa = .96 ± .01). For all subsequent tests, accuracy values were averaged between the raters. Mean accuracy for each condition is shown in Figure 2a. As expected, accuracy was higher for intact (mean = 98.33 ± 0.80%) compared to locally scrambled (mean = 20.20 ± 2.54%) and globally scrambled images (mean = 3.35 ± 0.82%). A one-way repeated measures ANOVA revealed a significant main effect of scrambling ($F(2,34) = 374.76$, $p < .001$, generalized-$\eta^2 = .95$). A series of post-hoc t-tests revealed significantly higher accuracies for intact compared to locally scrambled scenes, intact compared to globally scrambled scenes, and locally scrambled compared to globally scrambled scenes (all $p < .001$). For trials where descriptive responses were given, participants also provided confidence ratings of their descriptions on a scale of 1 (not at all confident) to 7 (very confident). Median ratings for each condition were calculated for each participant and are shown in Figure 3b. One participant's data were excluded from the analysis as they provided no responses, and hence no confidence ratings, for the scrambled images. Similar to accuracy, confidence ratings were higher for intact (median = 7, IQR = 6 - 7) compared to locally scrambled (median = 2, IQR = 2 - 3) and globally scrambled images (median = 2, IQR = 1 - 2). A Friedman's ANOVA revealed a significant main effect of scrambling ($\chi^2(2) = 31.60$, $p < .001$). A series of post-hoc Wilcoxon signed-rank tests revealed significantly higher confidence ratings for intact than locally scrambled scenes ($p < .001$), intact than globally

scrambled scenes (p < .001), and locally scrambled than globally scrambled scenes (p = .004). Thus both types of scrambling significantly impaired participants' recognition and confidence on a scene recognition test.

[Figure 2 near here]

Scene Decoding Analysis

Next, we used fMRI to measure the patterns of neural response to each of the conditions. The group normalised responses within the PPA, RSC, and OPA regions are shown in Supplementary Figure 4 (red and blue colours indicate responses above and below the mean respectively). Correlation-based MVPA (Haxby et al., 2001) using a leave-one-participant-out (LOPO) cross-validation scheme was then used to assess the reliability of these responses. Average correlation similarity matrices for each of the ROIs and each of the scrambling types are shown in Figure 3, with symmetrically opposite points averaged across the diagonal to aid visualisation.

[Figure 3 near here]

We first assessed the ability of the MVPA to decode the scene categories under each of the levels of scrambling. We calculated within- and between-category correlation values averaged across categories for each scrambling type and ROI. These values are shown in Figure 4. Paired-samples t-tests were then used to test for differences between within- and between-category correlations; if categories can be decoded based on patterns of brain activity, then significantly greater within- than between-category correlations would be expected. For the intact scenes, significantly greater within- than between-category correlations were observed in the PPA ($t(19) = 10.90$, p < .001, Cohen's d = 2.44) and OPA

(t(19) = 9.89, p < .001, Cohen's d = 2.21), but not in the RSC (t(19) = 0.17, p > .999, Cohen's d = 0.04). In the locally scrambled condition, significantly greater within- than between-category correlations were found in the PPA (t(19) = 5.54, p < .001, Cohen's d = 1.24) and OPA (t(19) = 4.57, p = .001, Cohen's d = 1.02), but not in the RSC (t(19) = 1.43, p = .498, Cohen's d = 0.32). For the globally scrambled scenes, no significant differences were seen for any ROI (PPA: t(19) = 0.43, p > .999, Cohen's d = 0.10; RSC: t(19) = 2.20, p = .200, Cohen's d = 0.49; OPA: t(19) = 2.14, p = .200, Cohen's d = 0.48).

A further test of the similarity in response between scrambling conditions is the extent to which neural response patterns generalise across them. This was tested using cross-decoding analyses. MVP analyses were conducted in which the neural response patterns to intact scenes were now correlated with the neural response patterns to 1) the locally scrambled scenes, and 2) the globally scrambled scenes. If response patterns to a given scene category remain similar across the scrambling conditions, then significant decoding of the scene categories from these cross-condition MVP analyses would be expected. The results of these cross-decoding analyses are shown in Supplementary Figure 7. The comparison of intact and locally scrambled scenes revealed significant decoding of scene category in the PPA (t(19) = 8.13, p < .001, Cohen's d = 1.82) and OPA (t(19) = 7.13, p < .001, Cohen's d = 1.59), but not the RSC (t(19) = 1.08, p = .583, Cohen's d = 0.24). Similarly, the comparison of intact and globally scrambled scenes also revealed significant decoding of scene category in the PPA (t(19) = 5.62, p < .001, Cohen's d = 1.26) and OPA (t(19) = 5.82, p < .001, Cohen's d = 1.30), but not the RSC (t(19) = 0.45, p = .655, Cohen's d = 0.10). Thus, response patterns in PPA and OPA generalised well between intact and locally scrambled, and intact and globally scrambled conditions.

[Figure 4 near here]

Representational Similarity Analysis

We next conducted a series of representational similarity analyses (RSAs; Kriegeskorte et al., 2008) to test to what extent the two types of scrambling influence the representational structure of the responses relative to those of the intact scenes. The off-diagonal elements of the group average matrices (20 elements per matrix) were correlated between intact and locally scrambled conditions, and intact and globally scrambled conditions. If the scrambling does not disrupt the representational space, a significant positive correlation would be expected with the intact scenes matrix. A significant positive correlation was observed between intact and locally scrambled scenes in the PPA ($r(18) = .66$, $p = .009$), but not in the OPA ($r(18) = -.15$, $p > .999$), whilst a significant negative correlation was observed in the RSC ($r(18) = -.56$, $p = .044$). A significant positive correlation was observed between intact and globally scrambled conditions in the OPA($r(18) = .62$, $p = .019$), but not the PPA ($r(18) = .44$, $p = .160$)or RSC($r(18) = .02$, $p > .999$). These results are illustrated in Figure 5 (see also Supplementary Figure 6).

[Figure 5 near here]

To further quantify the degree of preserved pattern similarity under scrambling we undertook an additional analysis of representational similarity, taking into account individual variation and the distribution of correlations this entails (Supplementary Figure 7). Such variation leads to a "noise ceiling" (Nili et al., 2014), i.e., an upper bound to the observable correlation between intact and scrambled conditions. By comparing the observed correlations with the noise ceiling, we can determine the degree to which preserved representational structure under scrambled conditions accounts for the

explicable variance in the data. This approach also permits a more sensitive comparison with a zero correlation, which would be expected if scrambling abolished the representational structure for intact images.

The noise ceiling is estimated by correlating each LOPO iteration's intact similarity matrix against the group average intact similarity matrix (calculated across all LOPO iterations for the noise ceiling upper bound, and across all LOPO iterations but the current one for the noise ceiling lower bound), and then averaging these correlations. This reflects the maximum similarity that could be expected for any correlation between the intact and scrambled conditions. Noise ceilings were reasonably high in the PPA and OPA indicating a good degree of reliability in the intact responses across LOPO iterations, but were much closer to zero in the RSC indicating relatively poor reliability in this region.

Next, we calculated the correlation between each LOPO iteration's locally- or globally-scrambled similarity matrix and the group average intact similarity matrix. A one-sample t-test was used to contrast each of these correlation distributions against zero. For the comparison of intact and locally scrambled conditions, correlations were significantly greater than zero in the PPA ($t(19) = 7.44$, $p < .001$, Cohen' d = 1.66), significantly less than zero in the RSC ($t(19) = 3.17$, $p = .015$, Cohen's d = 0.71), and less than zero in the OPA with the difference approaching significance ($t(19) = 2.41$, $p = .053$, Cohen' d = 0.54). For the comparison of intact and globally scrambled conditions, correlations were significantly greater than zero in the PPA ($t(19) = 5.51$, $p < .001$, Cohen's d = 1.23) and OPA ($t(19) = 8.83$, $p < .001$, Cohen's d = 1.97), and did not differ significantly from zero in the RSC ($t(19) = 0.09$, $p = .929$, Cohen's d = 0.02). Next, we compared the correlations with the noise ceiling. For the comparison of intact and locally scrambled conditions, correlations were significantly

399 below the lower bound of the noise ceiling in the RSC ($t(19) = 5.00$, $p < .001$, Cohen's $d = 1.12$) and OPA ($t(19) = 14.69$, $p < .001$, Cohen's $d = 3.28$), but not the PPA ($t(19) = 1.70$, $p = .211$, Cohen's $d = 0.38$). For the comparison of intact and globally scrambled conditions, correlations were significantly below the lower bound of the noise ceiling in the PPA ($t(19) = 5.89$, $p < .001$, Cohen's $d = 1.32$) and OPA ($t(19) = 2.97$, $p = .023$, Cohen's $d = 0.66$), but not the RSC ($t(19) = 1.21$, $p = .241$, Cohen's $d = 0.27$). This shows that in most cases the local and global scrambling conditions ability to predict the intact responses fell significantly below the theoretical maximum of the noise ceiling. Overall, this analysis demonstrates that, for PPA and OPA, significant representational structure is preserved under even global scrambling conditions although it also shows that other sources of variance play a role.

409 We next tested the extent to which the definition of the scene ROIs influenced the MVPA results. The main scene ROIs were defined using a contrast of Scenes > Phase Scrambled versions of those scenes. We defined an alternative set of ROIs for the main scene regions (PPA, RSC, OPA) from independent localiser data of separate experiments (not reported here) using contrasts of Scenes > Faces and Scenes > Objects. The locations of these ROIs are illustrated in Supplementary Figure 8, and co-ordinates of the corresponding peak voxels are given in Supplementary Table 2. Locations of the PPA and RSC regions remained relatively consistent across the definitions (cf. Table 1 and Supplementary Figure 3). We next repeated our MVP analyses for these alternative ROIs. Results of the decoding analyses were largely consistent with those for the main ROIs (Supplementary Figure 9; cf. Figure 4). Representational similarity analyses remained broadly consistent between the main and alternative definitions (Supplementary Figure 10; cf. Figure 5).

In order to interpret the results of representational similarity analyses within scene selective regions, it is essential to identify any disruption of earlier stages of visual processing. To test whether category specific visual responses in early visual cortex survive scrambling of low-level image properties, we repeated our analyses in a V1 control region defined using a probabilistic atlas (Wang et al., 2015). The results of this analysis are shown in Supplementary Figure 11. Paired-samples t-tests revealed significantly higher within- than between-category correlations for the intact ($t(19) = 7.82$, $p < .001$, Cohen's $d = 1.75$), locally scrambled ($t(19) = 4.28$, $p < .001$, Cohen's $d = 0.96$), and globally scrambled scenes ($t(19) = 4.68$, $p < .001$, Cohen's $d = 1.05$). Representational similarity analyses revealed a significant correlation between the intact and globally scrambled conditions ($r(18) = .71$, $p = .001$), but not between intact and locally scrambled conditions ($r(18) = .37$, $p = .112$). Overall, these results indicate that preserved low-level features are sufficient to maintain reliable spatial patterns of response in V1 after scrambling.

Finally, we repeated our analyses using a whole-brain searchlight approach to identify areas beyond our regions of interest where patterns of response to intact and scrambled images are systematically affected by stimulus category. The results of these analyses are plotted on the cortical surface in Supplementary Figure 12. Spheres showing significant decoding of category for intact scenes were observed throughout occipital and ventro-temporal cortices. Decoding for the scrambled scene conditions was less widespread; nevertheless, significant spheres were observed in right ventro-temporal cortices and some occipital regions for locally scrambled scenes, and in some occipital regions for globally scrambled scenes. Representational similarity analyses revealed significant spheres in regions including ventro-temporal and occipital cortices, both for the

444 comparison of intact and locally scrambled scenes, and intact and globally scrambled
445 scenes.

446

DISCUSSION

The aim of the present study was to directly determine whether category-selective patterns of response in scene-selective regions can be explained by the visual properties of the stimulus. To address this issue, we compared patterns of response to intact and scrambled images. Our hypothesis was that, if category-selective patterns of response purely reflect the semantic content of the images, there should be little similarity between the patterns of response elicited by intact and scrambled images. On the other hand, if category-specific patterns are based on visual properties, similar patterns should be elicited by both intact and scrambled images. Image scrambling significantly impaired the ability to categorize scenes, consistent with previous results showing that local phase information is important for recognition of scene *gist* (Loschky et al., 2007). However, we found distinct and reliable category-selective patterns of response for both the intact and scrambled image conditions in the PPA and OPA scene-selective regions. Moreover, the patterns of response elicited by intact scenes were similar to the patterns of response to scrambled scenes.

Previous studies have identified distinct patterns of neural response to different categories of scene in scene selective regions (Walther et al., 2009, 2011; Watson et al., 2014). Our results show that categorical patterns of response in scene-selective regions are still evident to images with significantly reduced semantic information. These findings are consistent with recent studies in which we have shown that basic image properties of different scene categories can predict patterns of response in scene-selective regions (Rice, Watson, Hartley, & Andrews, 2014; Watson et al., 2014, 2016). However, because images drawn from the same category are likely to have similar visual properties (Oliva & Torralba, 2001), it was unclear from this previous work whether or not patterns are determined

primarily by categorical or visual properties of the image. The results from the current study provide more direct evidence that lower-level visual properties of the image can account for a substantial proportion of the variance in the patterns of response in scene-selective regions. This does not dispute that there are distinct patterns of response to different scene categories in scene-selective regions, but rather suggests that such effects may be underpinned, at least in part, by sensitivity to the visual properties of scenes.

To evaluate the importance of spatial properties in the neural representation of scenes, we compared scrambling across the full global extent of the image, or independently within local windows of the image. The local scrambling thus preserves the coarse-scale global structure of the original image more than the global scrambling, in the sense that the local scrambling leaves the windows of the grid in their original spatial positions (see also Figure 1 & Supplementary Figure 1). In PPA, we found that responses could be discriminated for locally scrambled scenes, but the ability to discriminate globally scrambled images was less reliable. Furthermore, a representational similarity analysis showed that local scrambling preserved the pattern of response to intact images more than globally scrambling. This would suggest that the PPA is sensitive to the coarse-scale spatial organisation of the image, such that responses are disrupted more by global scrambling. Such a conclusion would be consistent with previous studies demonstrating sensitivity of the PPA to the spatial structure of scenes (Epstein, Higgins, Parker, Aguirre, & Cooperman, 2006; Kravitz et al., 2011; Park et al., 2011), and displaying visual field biases (Arcaro et al., 2009; Cichy et al., 2013; Silson et al., 2015). Indeed, it has been proposed that the PPA may support extraction of local spatial geometries of the scene (Epstein, 2008; Epstein, Parker, & Feiler, 2007), for which local visual features may be important.

There was a reduction in the magnitude of the category effect for scrambled scenes relative to intact scenes, suggesting that the scrambling process introduced some disruption to the neural representations. This suggests that patterns of response are dependent on higher-level information about the scene that is only available from the intact images. One possibility is that this higher-level information reflects the semantic or categorical properties conveyed by the image. For example, our noise ceiling analysis suggests that while significant pattern similarity is preserved, a substantial component is disrupted, particularly by global scrambling. However, an alternative possibility is that unexplained variance might reflect image properties that are disrupted by the scrambling process. An important feature of intact images is the strong statistical dependencies between features, such as location-specific combinations of orientation and spatial frequency. Indeed, the behavioural sensitivity to the regularities that occur in intact objects suggests that these properties are critical for differentiating between different classes of images (Loschky et al., 2007, 2010). It is possible that these properties also contribute to the patterns of response in scene-selective regions. When evaluating these possibilities, it is important to recognize that high- and low-level contributions to the observed representational structure are not mutually exclusive. The extraction of any high-level features depends on the availability of relevant low-level features preserved in the scrambled stimuli.

We found that category responses in the OPA could be discriminated for intact scenes and locally scrambled scenes, but not globally scrambled scenes. However, in contrast to the PPA the representational structure of the intact scenes was maintained by the global scrambling. Although the OPA has been causally implicated in the perception of scenes (Dilks et al., 2013; Ganaden, Mullin, & Steeves, 2013), its precise functional

properties are less well established than other scene regions. The greater similarity between intact and globally scrambled images suggests that the OPA is sensitive to global visual statistics, such as the texture of the image. Interestingly, this implies a possible functional distinction between PPA and OPA, with the PPA more clearly tuned to the local visual features than the OPA. Recent studies have reported a double dissociation in visual field biases between the PPA and OPA (Silson et al., 2015; Silson, Groen, Kravitz, & Baker, 2016), suggesting inputs to these regions may at least partially function in parallel rather than in series, and which may therefore support some degree of functional dissociation between them.

In contrast to the PPA and OPA, responses in RSC failed to discriminate the scene categories in any of the conditions. The representational similarity analyses showed that neither local nor global scrambling maintained the representational structure relative to the intact scenes. It has been proposed that the RSC may play a role representing the scene as part of the wider spatial environment (Epstein, 2008; Epstein et al., 2007) playing a crucial role in spatial memory, navigation and imagery – for example, translating between ego- and allocentric spatial representations (Byrne, Becker, & Burgess, 2007; Vann, Aggleton, & Maguire, 2009). Such processes suggest a more abstract form of representation, less directly tied to image features.

We also examined the response patterns within a V1 control region (Wang et al., 2015). We would expect this region to display sensitivity to the visual features of the scenes, but would be less likely to be modulated by higher-level semantic features of the scene categories. We observed significant decoding of the scene categories under all of the different scrambling conditions, consistent with the reliable differences in visual features

between different scene categories. We also observed a significant association between the patterns in the intact and globally scrambled conditions, consistent with the presence of the shared global visual features between the intact and globally scrambled conditions.

In conclusion, our results demonstrate distinct responses to different categories of scenes even when the perception of scene category is severely impaired by phase scrambling. These results should not be taken to imply that perception of scene category is independent of the neural response in scene-selective regions, but they do suggest that the topographic organization of regions such as the PPA and, to a lesser extent, the OPA can be explained by selectivity for the visual properties of the image.

548 **REFERENCES**

549 Aguirre, G. K., & D'Esposito, M. (1999). Topographical disorientation: a synthesis and
550 taxonomy. *Brain*, *122*(9), 1613–1628. http://doi.org/10.1093/brain/122.9.1613

551 Aguirre, G. K., Zarahn, E., & D'Esposito, M. (1998). An area within human ventral cortex
552 sensitive to "building" stimuli: evidence and implications. *Neuron*, *21*(2), 373–83.
553 Retrieved from http://www.ncbi.nlm.nih.gov/pubmed/9728918

554 Amit, E., Mehoudar, E., Trope, Y., & Yovel, G. (2012). Do object-category selective regions in
555 the ventral visual stream represent perceived distance information? *Brain and*
556 *Cognition*, *80*(2), 201–213. http://doi.org/10.1016/j.bandc.2012.06.006

557 Andrews TJ, Clarke A, Pell P & Hartley T (2010) Selectivity for low-level features of objects in
558 the human ventral stream. Neuroimage 49: 703-711.

559 Andrews, T. J., Watson, D. M., Rice, G. E., & Hartley, T. (2015). Low-level properties of
560 natural images predict topographic patterns of neural response in the ventral visual
561 pathway visual pathway. *Journal of Vision*, *15*(7), 1–12.
562 http://doi.org/10.1167/15.7.3.doi

563 Arcaro, M. J., McMains, S. A., Singer, B. D., & Kastner, S. (2009). Retinotopic Organization of
564 Human Ventral Visual Cortex. *Journal of Neuroscience*, *29*(34), 10638–10652.
565 http://doi.org/10.1523/jneurosci.2807-09.2009

566 Byrne, P., Becker, S., & Burgess, N. (2007). Remembering the past and imagining the future:
567 A neural model of spatial memory and imagery. *Psychological Review*, *114*(2), 340–375.
568 http://doi.org/10.1037/0033-295X.114.2.340

569 Cichy, R. M., Sterzer, P., Heinzle, J., Elliott, L. T., Ramirez, F., & Haynes, J.-D. (2013). Probing
570 principles of large-scale object representation: Category preference and location
571 encoding. *Human Brain Mapping*, *34*(7), 1636–1651.
572 http://doi.org/10.1002/hbm.22020

573 Coggan, D. D., Liu, W., Baker, D. H., & Andrews, T. J. (2016). Category-selective patterns of
574 neural response in the ventral visual pathway in the absence of categorical
575 information. *NeuroImage*, *135*, 107–114. http://doi.org/10.1167/15.12.622

576 Dilks, D. D., Julian, J. B., Kubilius, J., Spelke, E. S., & Kanwisher, N. (2011). Mirror-Image
577 Sensitivity and Invariance in Object and Scene Processing Pathways. *Journal of*
578 *Neuroscience*, *31*(31), 11305–11312. http://doi.org/10.1523/jneurosci.1935-11.2011

579 Dilks, D. D., Julian, J. B., Paunov, A. M., & Kanwisher, N. (2013). The Occipital Place Area Is
580 Causally and Selectively Involved in Scene Perception. *Journal of Neuroscience*, *33*(4),
581 1331–1336. http://doi.org/10.1523/JNEUROSCI.4081-12.2013

582 Epstein, R. A. (2008). Parahippocampal and retrosplenial contributions to human spatial
583 navigation. *Trends in Cognitive Sciences*, *12*(10), 388–396.
584 http://doi.org/10.1016/j.tics.2008.07.004

585 Epstein, R. A., Graham, K. S., & Downing, P. E. (2003). Viewpoint-specific scene
586 representations in human parahippocampal cortex. *Neuron*, *37*(5), 865–876.
587 http://doi.org/10.1016/s0896-6273(03)00117-x

588 Epstein, R. A., Harris, A., Stanley, D., & Kanwisher, N. (1999). The parahippocampal place
589 area: Recognition, navigation, or encoding? *Neuron*, *23*(1), 115–125.
590 http://doi.org/10.1016/s0896-6273(00)80758-8

591 Epstein, R. A., & Higgins, J. S. (2007). Differential parahippocampal and retrosplenial
592 involvement in three types of visual scene recognition. *Cerebral Cortex*, *17*(7), 1680–
593 1693. http://doi.org/10.1093/cercor/bhl079

594 Epstein, R. A., Higgins, J. S., Parker, W., Aguirre, G. K., & Cooperman, S. (2006). Cortical
595 correlates of face and scene inversion: A comparison. *Neuropsychologia*, *44*(7), 1145–
596 1158. http://doi.org/10.1016/j.neuropsychologia.2005.10.009

597 Epstein, R. A., & Kanwisher, N. (1998). A cortical representation of the local visual
598 environment. *Nature*, *392*(6676), 598–601. http://doi.org/10.1038/33402

599 Epstein, R. A., Parker, W. E., & Feiler, A. M. (2007). Where am I now? Distinct roles for
600 parahippocampal and retrosplenial cortices in place recognition. *Journal of*
601 *Neuroscience*, *27*(23), 6141–6149. http://doi.org/10.1523/jneurosci.0799-07.2007

602 Ganaden, R. E., Mullin, C. R., & Steeves, J. K. E. (2013). Transcranial Magnetic Stimulation to
603 the Transverse Occipital Sulcus Affects Scene but Not Object Processing. *Journal of*
604 *Cognitive Neuroscience*, *25*(6), 961–968. http://doi.org/10.1162/jocn

605 Golomb, J. D., & Kanwisher, N. (2012). Higher Level Visual Cortex Represents Retinotopic,
606 Not Spatiotopic, Object Location. *Cerebral Cortex*, *22*(12), 2794–2810.
607 http://doi.org/10.1093/cercor/bhr357

608 Groen, I. I. A., Silson, E. H. & Baker, C. I. (2017) Contributions of low- and high-level
609 properties to neural processing of visual scenes in the human brain. *Philos. Trans. R.*
610 *Soc. B* 1–22. doi:10.1098/rstb.2016.0102

611 Hanke, M., Halchenko, Y. O., Sederberg, P. B., Hanson, S. J., Haxby, J. V, & Pollmann, S.
612 (2009). PyMVPA: a Python Toolbox for Multivariate Pattern Analysis of fMRI Data.
613 *Neuroinformatics*, *7*(1), 37–53. http://doi.org/10.1007/s12021-008-9041-y

614 Hasson, U., Harel, M., Levy, I., & Malach, R. (2003). Large-scale mirror-symmetry
615 organization of human occipito-temporal object areas. *Neuron*, *37*(6), 1027–1041.
616 http://doi.org/10.1016/s0896-6273(03)00144-2

617 Haxby, J. V, Connolly, A. C., & Guntupalli, J. S. (2014). Decoding Neural Representational
618 Spaces Using Multivariate Pattern Analysis. *Annual Review of Neuroscience*, *37*, 435–
619 456. http://doi.org/10.1146/annurev-neuro-062012-170325

620 Haxby, J. V, Gobbini, M., Furey, M., Ishai, A., Schouten, J., & Pietrini, P. (2001). Distributed
621 and overlapping representations of faces and objects in ventral temporal cortex.
622 *Science*, *293*(5539), 2425–2430. http://doi.org/10.1126/science.1063736

623 Henderson, J. M., Zhu, D. C., & Larson, C. L. (2011). Functions of parahippocampal place area
624 and retrosplenial cortex in real-world scene analysis: An fMRI study. *Visual Cognition*,
625 *19*(7), 910–927. http://doi.org/10.1080/13506285.2011.596852

626 Huth, A. G., Nishimoto, S., Vu, A. T., & Gallant, J. L. (2012). A Continuous Semantic Space
627 Describes the Representation of Thousands of Object and Action Categories across the
628 Human Brain. *Neuron*, *76*(6), 1210–1224. http://doi.org/10.1016/j.neuron.2012.10.014

Jenkinson, M., Bannister, P., Brady, M., & Smith, S. (2002). Improved Optimization for the Robust and Accurate Linear Registration and Motion Correction of Brain Images. *NeuroImage*, *17*(2), 825–841. http://doi.org/10.1006/nimg.2002.1132

Julian, J. B., Fedorenko, E., Webster, J., & Kanwisher, N. (2012). NeuroImage An algorithmic method for functionally defining regions of interest in the ventral visual pathway. *NeuroImage*, *60*(4), 2357–2364. http://doi.org/10.1016/j.neuroimage.2012.02.055

Köhler, S., Crane, J., & Milner, B. (2002). Differential contributions of the parahippocampal place area and the anterior hippocampus to human memory for scenes. *Hippocampus*, *12*(6), 718–723. http://doi.org/10.1002/hipo.10077

Kravitz, D. J., Peng, C. S., & Baker, C. I. (2011). Real-World Scene Representations in High-Level Visual Cortex: It's the Spaces More Than the Places. *Journal of Neuroscience*, *31*(20), 7322–7333. http://doi.org/10.1523/jneurosci.4588-10.2011

Kriegeskorte, N., Goebel, R., & Bandettini, P. (2006). Information-based functional brain mapping. *Proceedings of the National Academy of Sciences*, *103*(10), 3863–3868. http://doi.org/10.1073/pnas.0600244103

Kriegeskorte, N., Mur, M., & Bandettini, P. A. (2008). Representational similarity analysis - connecting the branches of systems neuroscience. *Frontiers in Systems Neuroscience*, *2*(4), 1–28. http://doi.org/10.3389/neuro.06.004.2008

Lescroart, M. D., Stansbury, D. E., & Gallant, J. L. (2015). Fourier power, subjective distance, and object categories all provide plausible models of BOLD responses in scene-selective visual areas. *Frontiers in Computational Neuroscience*, *9*. http://doi.org/10.3389/fncom.2015.00135

Levy, I., Hasson, U., Avidan, G., Hendler, T., & Malach, R. (2001). Center – periphery organization of human object areas. *Nature Neuroscience*, *4*(5), 533–539.

Levy, I., Hasson, U., Harel, M., & Malach, R. (2004). Functional analysis of the periphery effect in human building-related areas. *Human Brain Mapping*, *22*(1), 15–26. http://doi.org/10.1002/hbm.20010

Loschky, L. C., Hansen, B. C., Sethi, A., & Pydimarri, T. N. (2010). The role of higher order image statistics in masking scene gist recognition. *Attention, Perception, & Psychophysics*, *72*(2), 427–444. http://doi.org/10.3758/APP.72.2.427

Loschky, L. C., Sethi, A., Simons, D. J., Pydimarri, T. N., Ochs, D., & Corbeille, J. L. (2007). The importance of information localization in scene gist recognition. *Journal of Experimental Psychology: Human Perception and Performance*, *33*(6), 1431–1450. http://doi.org/10.1037/0096-1523.33.6.1431

Maguire, E. (2001). The retrosplenial contribution to human navigation: A review of lesion and neuroimaging findings. *Scandinavian Journal of Psychology*, *42*(3), 225–238. http://doi.org/10.1111/1467-9450.00233

Mendez, M. F., & Cherrier, M. M. (2003). Agnosia for scenes in topographagnosia. *Neuropsychologia*, *41*(10), 1387–1395. http://doi.org/10.1016/s0028-3932(03)00041-1

Mullally, S. L., & Maguire, E. A. (2011). A new role for the parahippocampal cortex in representing space. *The Journal of Neuroscience*, *31*(20), 7441–9.

http://doi.org/10.1523/JNEUROSCI.0267-11.2011

Musel, B., Kauffmann, L., Ramanoël, S., Giavarini, C., Guyader, N., Chauvin, A., & Peyrin, C. (2014). Coarse-to-fine Categorization of Visual Scenes in Scene-selective Cortex. *Journal of Cognitive Neuroscience*, *26*(10), 2287–2297. http://doi.org/10.1162/jocn

Nasr, S., Echavarria, C. E., & Tootell, R. B. H. (2014). Thinking Outside the Box: Rectilinear Shapes Selectively Activate Scene-Selective Cortex. *Journal of Neuroscience*, *34*(20), 6721–6735. http://doi.org/10.1523/JNEUROSCI.4802-13.2014

Nasr, S., & Tootell, R. B. H. (2012). A cardinal orientation bias in scene-selective visual cortex. *The Journal of Neuroscience*, *32*(43), 14921–6. http://doi.org/10.1523/JNEUROSCI.2036-12.2012

O'Craven, K. M., & Kanwisher, N. (2000). Mental imagery of faces and places activates corresponding stiimulus-specific brain regions. *Journal of Cognitive Neuroscience*, *12*(6), 1013–23. Retrieved from http://www.ncbi.nlm.nih.gov/pubmed/11177421

Oliva, A., & Torralba, A. (2001). Modeling the Shape of the Scene: A Holistic Representation of the Spatial Envelope. *International Journal of Computer Vision*, *42*(3), 145–175. http://doi.org/10.1023/a:1011139631724

Op de Beeck, H. P. (2010). Against hyperacuity in brain reading: spatial smoothing does not hurt multivariate fMRI analyses? *NeuroImage*, *49*(3), 1943–8. http://doi.org/10.1016/j.neuroimage.2009.02.047

Park, S., Brady, T. F., Greene, M. R., & Oliva, A. (2011). Disentangling Scene Content from Spatial Boundary: Complementary Roles for the Parahippocampal Place Area and Lateral Occipital Complex in Representing Real-World Scenes. *Journal of Neuroscience*, *31*(4), 1333–1340. http://doi.org/10.1523/jneurosci.3885-10.2011

Park, S., Intraub, H., Yi, D.-J., Widders, D., & Chun, M. M. (2007). Beyond the Edges of a View: Boundary Extension in Human Scene-Selective Visual Cortex. *Neuron*, *54*(2), 335–342. http://doi.org/10.1016/j.neuron.2007.04.006

Park, S., Konkle, T., & Oliva, A. (2015). Parametric Coding of the Size and Clutter of Natural Scenes in the Human Brain. *Cerebral Cortex*, *25*, 1792–1805. http://doi.org/10.1093/cercor/bht418

Peirce, J. W. (2007). PsychoPy - Psychophysics software in Python. *Journal of Neuroscience Methods*, *162*, 8–13. http://doi.org/10.1016/j.jneumeth.2006.11.017

Peirce, J. W. (2009). Generating Stimuli for Neuroscience Using PsychoPy. *Frontiers in Neuroinformatics*, *2*(10), 1–8. http://doi.org/10.3389/neuro.11.010.2008

Poldrack, R. A., Halchenko, Y. O., & Hanson, S. J. (2009). Decoding the large-scale structure of brain function by classifying mental states across individuals. *Psychological Science*, *20*(11), 1364–72. http://doi.org/10.1111/j.1467-9280.2009.02460.x

Rajimehr, R., Devaney, K. J., Bilenko, N. Y., Young, J. C., & Tootell, R. B. H. (2011). The "Parahippocampal Place Area" Responds Preferentially to High Spatial Frequencies in Humans and Monkeys. *PLoS Biol*, *9*(4), e1000608. http://doi.org/10.1371/journal.pbio.1000608

Rice, G. E., Watson, D. M., Hartley, T., & Andrews, T. J. (2014). Low-level image properties of visual objects predict patterns of neural response across category-selective regions of the ventral visual pathway. *Journal of Neuroscience*, *34*(26), 8837–8844. Retrieved from http://www.jneurosci.org/content/34/26/8837.short

Schinazi, V. R., & Epstein, R. A. (2010). Neural correlates of real-world route learning. *Neuroimage*, *53*(2), 725–735. http://doi.org/10.1016/j.neuroimage.2010.06.065

Shinkareva, S. V, Mason, R. A., Malave, V. L., Wang, W., Mitchell, T. M., & Just, M. A. (2008). Using FMRI brain activation to identify cognitive states associated with perception of tools and dwellings. *PloS One*, *3*(1), e1394. http://doi.org/10.1371/journal.pone.0001394

Silson, E. H., Chan, a. W.-Y., Reynolds, R. C., Kravitz, D. J., & Baker, C. I. (2015). A Retinotopic Basis for the Division of High-Level Scene Processing between Lateral and Ventral Human Occipitotemporal Cortex. *Journal of Neuroscience*, *35*(34), 11921–11935. http://doi.org/10.1523/JNEUROSCI.0137-15.2015

Silson, E. H., Groen, I. I. A., Kravitz, D. J., & Baker, C. I. (2016). Evaluating the correspondence between face-, scene-, and object-selectivity and retinotopic organization within lateral occipitotemporal cortex. *Journal of Vision*, *16*(6), 14. http://doi.org/10.1167/16.6.14

Stansbury, D. E., Naselaris, T., & Gallant, J. L. (2013). Natural Scene Statistics Account for the Representation of Scene Categories in Human Visual Cortex. *Neuron*, *79*(5), 1025–1034. http://doi.org/10.1016/j.neuron.2013.06.034

Vann, S. D., Aggleton, J. P., & Maguire, E. a. (2009). What does the retrosplenial cortex do? *Nature Reviews Neuroscience*, *10*(11), 792–802. http://doi.org/10.1038/nrn2733

Walther, D. B., Caddigan, E., Fei-Fei, L., & Beck, D. M. (2009). Natural Scene Categories Revealed in Distributed Patterns of Activity in the Human Brain. *Journal of Neuroscience*, *29*(34), 10573–10581. http://doi.org/10.1523/jneurosci.0559-09.2009

Walther, D. B., Chai, B., Caddigan, E., Beck, D. M., & Fei-Fei, L. (2011). Simple line drawings suffice for functional MRI decoding of natural scene categories. *Proceedings of the National Academy of Sciences*, *108*(23), 9661–9666. http://doi.org/10.1073/pnas.1015666108

Wang, L., Mruczek, R. E., Arcaro, M. J., & Kastner, S. (2015). Probabilistic Maps of Visual Topography in Human Cortex. *Cerebral Cortex*, *25*(October), 3911–3931. http://doi.org/10.1093/cercor/bhu277

Watson, D. M., Hartley, T., & Andrews, T. J. (2014). Patterns of response to visual scenes are linked to the low-level properties of the image. *NeuroImage*, *99*, 402–410. http://doi.org/10.1016/j.neuroimage.2014.05.045

Watson, D. M., Hymers, M., Hartley, T., & Andrews, T. J. (2016). Patterns of neural response in scene-selective regions of the human brain are affected by low-level manipulations of spatial frequency. *NeuroImage*, *124*, 107–117. http://doi.org/10.1016/j.neuroimage.2015.08.058

Willenbockel, V., Sadr, J., Fiset, D., Horne, G. O., Gosselin, F., & Tanaka, J. W. (2010). Controlling low-level image properties: The SHINE toolbox. *Behavior Research Methods*,

42(3), 671–684. http://doi.org/10.3758/brm.42.3.671

Xiao, J. X., Hays, J., Ehinger, K. A., Oliva, A., & Torralba, A. (2010). SUN Database: Large-scale Scene Recognition from Abbey to Zoo. In *IEEE Conference on Computer Vision and Pattern Recognition* (pp. 3485–3492). Los Alamitos: IEEE Computer Soc. http://doi.org/10.1109/cvpr.2010.5539970

TABLES

Table 1. Peak MNI mm co-ordinates, voxel counts, and thresholds of standard scene selective clusters (PPA, RSC, OPA).

Region	Hemisphere	*x*	*y*	*z*	Voxel count	Threshold (Z)
PPA	L	-34	-46	-22	500	5.06
	R	26	-50	-18	500	5.59
RSC	L	-18	-52	-2	500	4.63
	R	16	-58	6	502	4.79
OPA	L	-36	-90	2	500	5.14
	R	38	-82	4	499	5.03

761 **FIGURES**

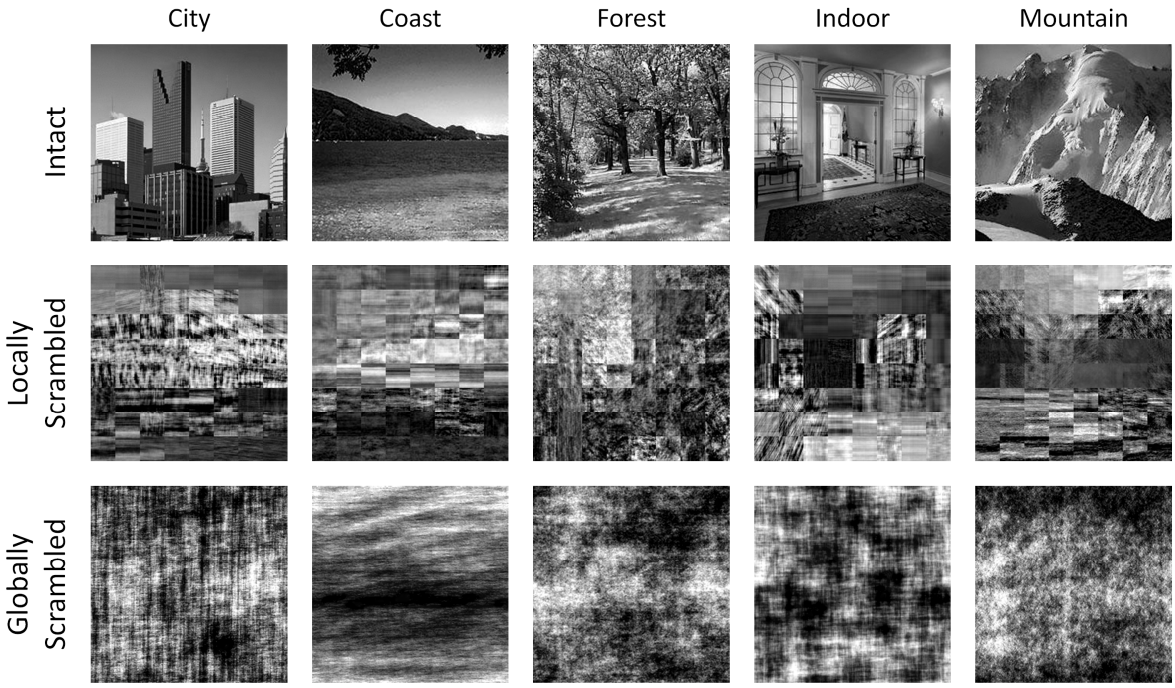

762

763 **Figure 1.** Examples of the scene images used in each condition.

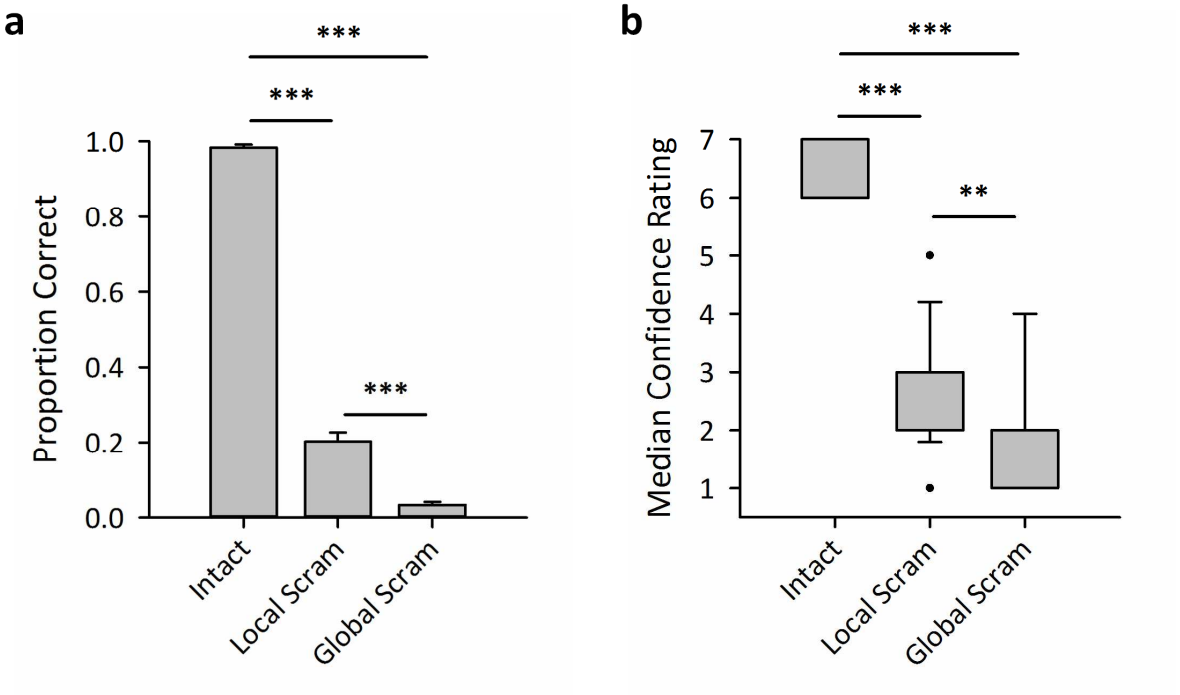

764

765 **Figure 2.** Results of the behavioural experiment. (a) Mean scene identification accuracies
766 for each level of scrambling. Error bars represents 1 SEM. (b) Box-plots of median
767 confidence ratings for each level of scrambling. (*** $p < .001$, ** $p < .01$, * $p < .05$).

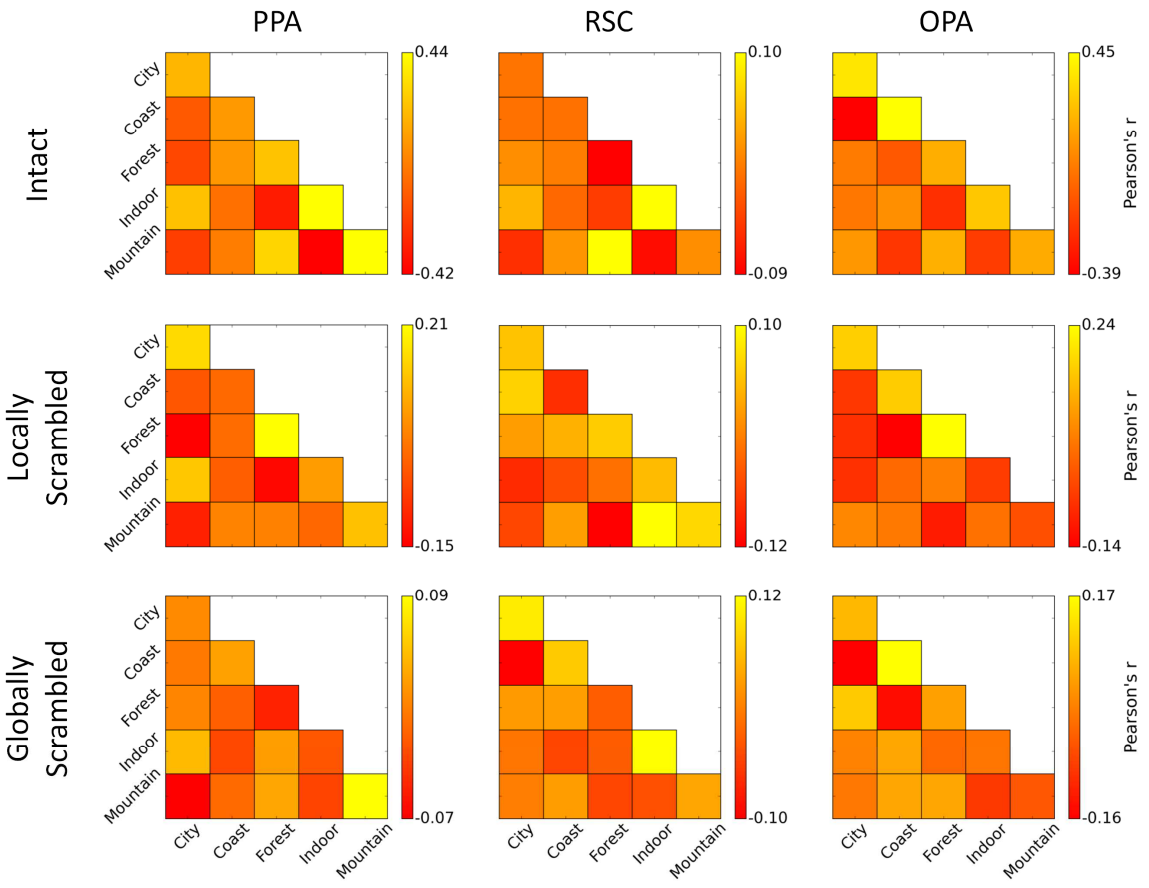

768

769 **Figure 3.** MVPA results: correlation similarity matrices for each level of scrambling in each

770 region of interest. To aid visualisation, symmetrically opposite points across the diagonal

771 have been averaged and displayed within the lower-triangle portion of the matrix only.

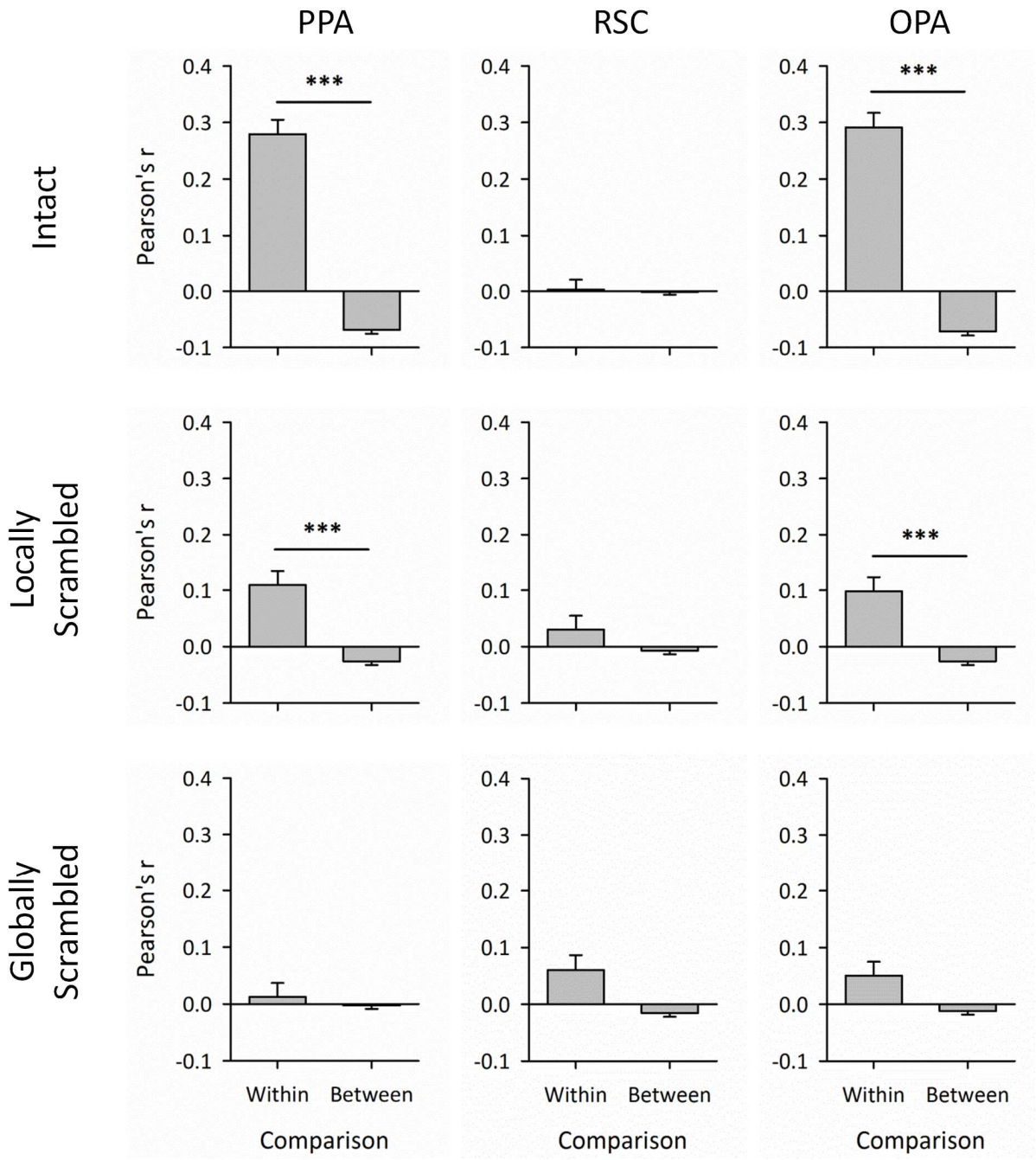

772

773 **Figure 4.** Decoding of categories from MVPA. Average within-category (on-diagonal) and
774 between-category (off-diagonal) values were calculated from the MVPA correlation
775 matrices. Significantly greater within- than between-category correlations indicate
776 categories can be successfully decoded. Error bar represent 1 SEM. (*** $p < .001$, ** $p <$
777 .01, * $p < .05$).

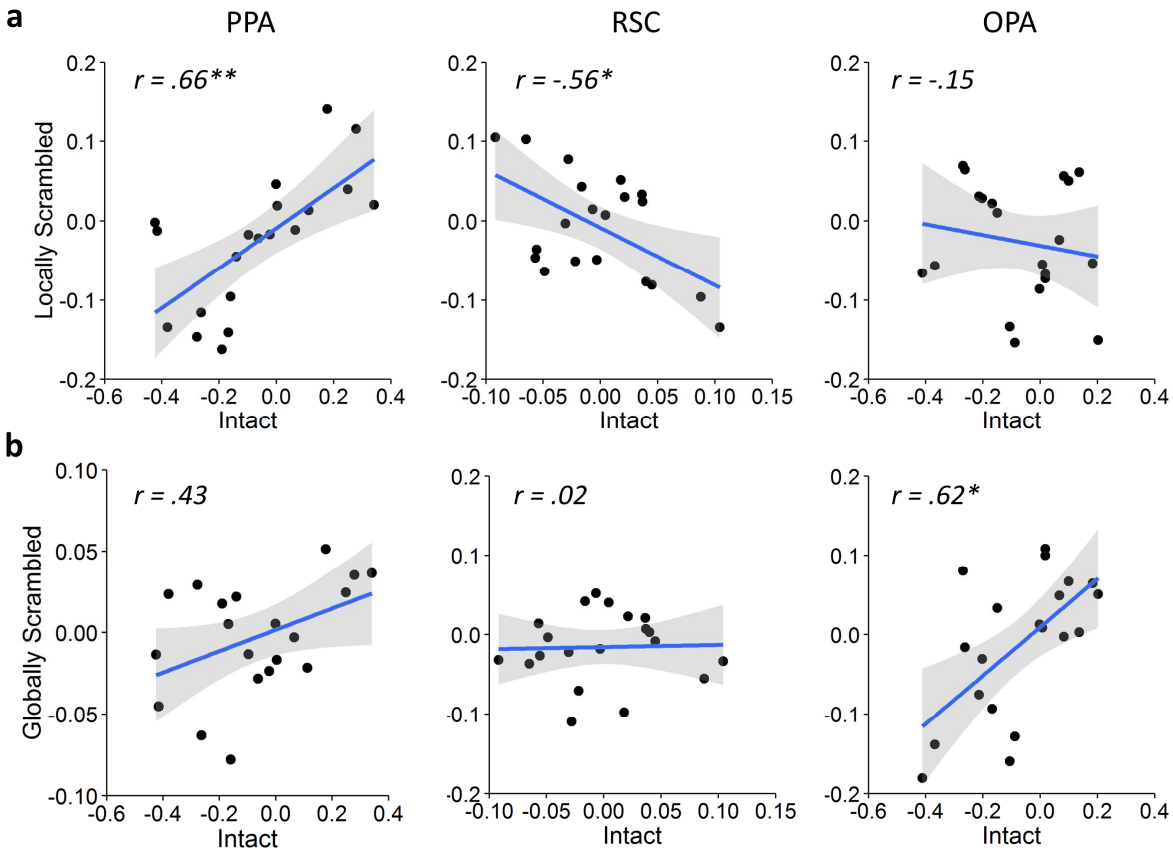

778

779 **Figure 5.** Representational similarity analyses. Off-diagonal elements of group average
780 MVPA correlation matrices (Figure 3) are correlated between (a) intact and locally-
781 scrambled conditions, and (b) intact and globally-scrambled conditions. Shaded regions
782 represent 95% confidence intervals. (*** $p < .001$, ** $p < .01$, * $p < .05$).

783

784